JACS
JOURNAL OF THE AMERICAN CHEMICAL SOCIETY
Article
pubs.acs.org/JACS

Origin of Enantioselectivity in the Propargylation of Aromatic Aldehydes Catalyzed by Helical *N*-Oxides

Tongxiang Lu,[‡] Rongxiu Zhu,[†,‡] Yi An,[‡] and Steven E. Wheeler*[,‡]

[‡]Department of Chemistry, Texas A&M University, College Station, Texas 77842, United States
[†]School of Chemistry and Chemical Engineering, Shandong University, Jinan, People's Republic of China

Supporting Information

ABSTRACT: The enantioselective propargylation of aromatic aldehydes with allenyltrichlorosilanes catalyzed by bipyridine *N*-oxides was explored using density functional theory. Low-lying transition states for a highly enantioselective helical bipyridine *N*-oxide catalyst [*Org. Lett.* **2011**, *13*, 1654] were characterized at the B97-D/TZV(2d,2p) level of theory. Predicted free energy barrier height differences are in agreement with experimental ee's for the propargylation of benzaldehyde and substituted analogues. The origin of enantioselectivity was pinpointed through distortion–interaction analyses. The stereoselectivity arises in part from through-space electrostatic interactions of the carbonyl carbon with the Cl ligands bound to Si, rather than noncovalent aryl–aryl interactions between the aromatic aldehyde and the helix as previously proposed. Moreover, aryl–aryl interactions between the aldehyde and helix are predicted to favor transition states leading to the *R* enantiomer, and ultimately reduce the enantioselectivity of this reaction. (*S*)-2,2′-bipyridine *N*-oxide was studied as a model catalyst in order to quantify the inherent enantioselectivity arising from different chiral arrangements of ligands around the hexacoordinate silicon in the stereocontrolling transition state for these reactions. The predicted selectivities arising from different chiral octahedral silicon complexes provide guidelines for the development of transition state models for *N*-oxide-based alkylation catalysts.

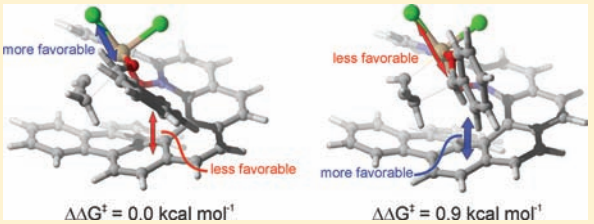

1. INTRODUCTION

Over the preceding decade, asymmetric organocatalysis has become one of the most rapidly developing areas in synthetic organic chemistry.[1] Of particular recent interest[2] has been the development of catalysts that exploit favorable noncovalent interactions (H-bonding, π-stacking interactions, etc.) to promote a given reaction pathway rather than relying on unfavorable steric interactions to hinder undesired pathways. In this way, small molecule catalyst can be designed that more closely mimic natural enzymes and can benefit from the long-range nature of these noncovalent interactions.[2] However, determining whether putative noncovalent interactions actually underlie observed selectivities for such catalysts is often nontrivial due to the subtle nature of many of these effects, particularly π-stacking interactions.[3] Unraveling the role of these interactions, and their impact on enantioselectivity in organocatalysis, can be aided by careful computational analyses of predicted transition state (TS) structures.[4]

Optically active homopropargylic alcohols provide an enticing synthetic target because of their utility in the synthesis of complex chiral molecules.[6] However, the development of enantioselective, metal-free catalysts for the propargylation of aldehydes remains a challenge. In particular, although there have been numerous *N*-oxide catalysts developed for the asymmetric allylation of aldehydes using allyltrichlorosilane,[7] as pioneered by Denmark and co-workers in the 1990s,[8] the development of analogous propargylation catalysts has lagged behind. Indeed, prior to 2011, there was only one published asymmetric propargylation catalyst utilizing allenyltrichlorosilane. This catalyst was reported by Nakajima and co-workers in 2002,[9] and provides relatively low yields and enantioselectivities in propargylations,[9] despite providing very high ee's for allylation reactions.[10] Furthermore, the source of stereoinduction in both allylations and propargylations catalyzed by *N*-oxides has eluded precise characterization. Computational analyses of the stereocontrolling transition states can be used to refine and inform proposed transition state models for these reactions. Ultimately, such information can facilitate the rational design of improved catalysts.[11]

Takenaka and co-workers[5] recently developed a catalytic transformation in which the enantioselective propargylation of aromatic aldehydes with allenyltrichlorosilane was achieved using the helical 2,2′-bipyridine *N*-oxide[12] **1** (see Scheme 1). This was the first highly enantioselective propargylation catalyst utilizing allenyltrichlorosilanes, and yields (S)-homopropargylic alcohols in 74–96% ee for a range of aromatic aldehydes. When run in dichloromethane, it is generally assumed that *N*-oxide-catalyzed alkylations follow the dissociative route depicted in Scheme 2.[13] The stereocontrolling step involves a chairlike transition state featuring a hexacoordinate silicon, in which both alkyl–aldehyde and aldehyde–silicon bonds are formed.[13d]

Received: September 30, 2011
Published: January 9, 2012

dx.doi.org/10.1021/ja209241n | *J. Am. Chem. Soc.* 2012, 134, 3095–3102

Scheme 1. Enantioselective Propargylation of Aromatic Aldehydes[5] with Allenyltrichlorosilane Catalyzed by 1 and 2[a]

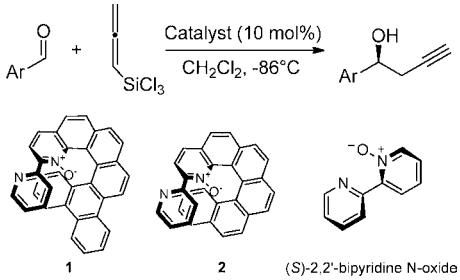

[a]Also included is (*S*)-2,2′-bipyridine *N*-oxide, which was used as a model of *N*-oxide catalysts.

Scheme 2. Catalytic Cycle for the Bipyridine *N*-Oxide-Catalyzed Propargylation of Aromatic Aldehydes Following a Dissociative Route

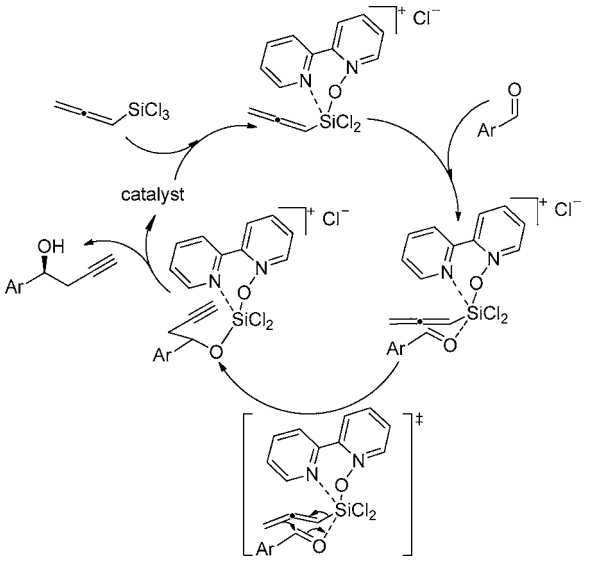

In propargylations catalyzed by **1**, Takenaka and co-workers[5] attributed the preference for *Si*-face attack in part to favorable π-stacking interactions between the aromatic aldehyde and the helix. *Re*-face addition was said to be hindered by steric interactions between the aldehyde and the terminal benzo unit of the helix (see Scheme 3). In this TS model,[5] the two

Scheme 3. Depiction of the TS Model of Takenaka and Co-workers (Nu = allene)[5]

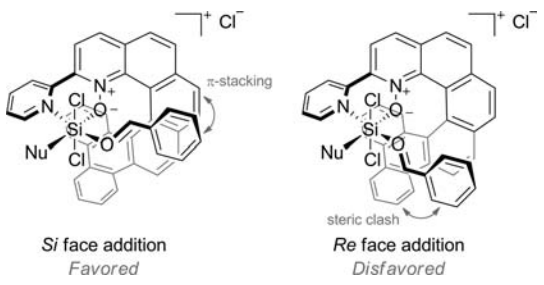

chlorines are in a *trans* arrangement, which is consistent with venerable stereoelectronic arguments regarding the preferred ligand arrangement of hexacoordinate silicon complexes.[14] These traditional arguments, which depend on the placement of the two electronegative chlorines in a *trans* configuration to facilitate the formation of a three-center, four-electron bond, have been used to rationalize myriad transition state models for *N*-oxide-catalyzed alkylations.[15] Similar arguments have motivated the placement of the alkyl nucleophile *trans* to the *N*-oxide in order to maximize nucleophile activation.[15] On the other hand, there have also been published transition state models for *N*-oxide catalysts that feature a *cis* arrangement of the two chlorines.[7g,x,13a] Thus, it remains an open question whether the chlorines adopt a *cis* or *trans* arrangement in the stereocontrolling transition states for these reactions. To our knowledge the only systematic computational investigation of the possible ligand arrangements of hexacoordinate silicon in the context of *N*-oxide-catalyzed reactions was published by Denmark and co-workers in 2005.[16] However, this study did not rule out the possibility of a *cis* arrangement of the chlorines. Also, these computations[16] were carried out at the semi-empirical PM3 level, which is known to often yield qualitatively incorrect predictions of enantioselectivities for organocatalyzed reactions.[17]

Below, (*S*)-2,2′-bipyridine *N*-oxide was studied as a model of *N*-oxide catalysts for the propargylation of benzaldehyde. This simplified system provides a way to examine the preferred coordination about the hexacoordinate silicon and the impact of this chiral environment on the enantioselectivity of propargylations. This is followed by more specific analyses of the propargylation of aromatic aldehydes catalyzed by the helical catalysts **1** and **2**, providing a simple explanation of the observed enantioselectivity.

2. THEORETICAL METHODS

All computations were performed at the B97-D/TZV(2d,2p) level of theory,[18] utilizing density fitting techniques. This dispersion-corrected DFT functional,[19] when paired with a triple-ζ basis set and density fitting, provides an effective yet computationally economical approach for organic reactions featuring noncovalent interactions.[20] In particular, B97-D is capable of capturing the dispersion effects that dominate the noncovalent interactions present while also accurately describing the transition states. For example, a recent study by Clark and co-workers demonstrated[17] excellent performance for the related ωB97xD approach in predicting enantioselectivities for organocatalyzed reactions. B97-D/TZV(2d,2p) is expected to perform similarly in this context.

Solvent effects (dichloromethane) were approximately accounted for using the PCM model.[21] Computations were carried out using Gaussian09,[22] and transitions states were characterized by the existence of a single imaginary vibrational frequency. All geometries and frequencies were computed using PCM, and gas phase energies were evaluated at solution-phase geometries. Ee's were evaluated on the basis of the solution-phase free energy barriers via

$$\mathrm{ee} = \frac{\sum_i e^{-\Delta G^{\ddagger}_{\mathrm{rel}}(S_i)/RT} - \sum_i e^{-\Delta G^{\ddagger}_{\mathrm{rel}}(R_i)/RT}}{\sum_i e^{-\Delta G^{\ddagger}_{\mathrm{rel}}(S_i)/RT} + \sum_i e^{-\Delta G^{\ddagger}_{\mathrm{rel}}(R_i)/RT}}$$

where $\Delta G^{\ddagger}_{\mathrm{rel}}(S_i)$, for example, is the free energy difference (relative to the lowest-lying TS) for the *i*th TS leading to the *S* product, *R* is the ideal gas constant, and T = 187 K. All transition states within 2 kcal mol^{-1} of the lowest-lying TS were included in the sums.

The energy differences between transition states were analyzed using the distortion−interaction approach of Houk and co-workers[23] (or, equivalently, the activation-strain model of Bickelhaupt et al.[24]). In such analyses of bimolecular reactions, barrier heights are decomposed into the energy required to distort each reactant to the TS geometry (E^{dist}) and the "interaction energy" between the distorted reactants in the TS ($E^{\mathrm{int}} = E^{\ddagger} - E^{\mathrm{dist}}$).

dx.doi.org/10.1021/ja209241n | J. Am. Chem. Soc. 2012, 134, 3095−3102

3. RESULTS AND DISCUSSION

3.1. Model (*S*)-Bipyridine *N*-Oxide Catalyst (BP). In order to quantify and clarify the impact of the hexacoordinate silicon intermediate on the enantioselectivity of *N*-oxide-catalyzed propargylation reactions, we have studied (*S*)-2,2′-bipyridine *N*-oxide as a model catalyst (see Scheme 2). These results can be used to guide the development of transition state models for these and related reactions, since this model system captures the dominant stereocontrolling center in these reactions.

For (*S*)-2,2′-bipyridine *N*-oxide bound to an octahedral silicon, there are 10 unique arrangements of the remaining ligands (allenyl group, aldehyde, and two chlorines) that are compatible with the addition of the allenyl group to the aldehyde. From each of these configurations, the allenyl group can add to the *Si* or *Re* face of the aldehyde, leading to formation of the *S* or *R* homopropargylic alcohol, respectively. B97-D predicted free energies for the 20 possible transition state structures [10 generating *R* enantiomers (shown in Figure 1) and 10 yielding *S* enantiomers] are presented in Figure 1. Free energies are reported relative to **BP1**(*R*).

Several salient features of these catalysts are revealed by this model system. First, the chiral arrangement of ligands about the octahedral silicon has a dramatic impact on predicted free energies and enantioselectivities. Second, the lowest-lying *R* and *S* transition states [**BP1**(R) and **BP1**(S)] correspond to a *trans* arrangement of the chlorines, in accord with traditional descriptions of octahedral silicon complexes.[14] However, **BP1**(S) and **BP1**(R) are nearly isoergonic, and this ligand arrangement is not expected to lead to stereoselectivity in the absence of other chiral elements. Third, in contrast to popular models,[5,15] in **BP1** the *N*-oxide is *trans* to the aldehyde, not the nucleophile (allenyl group). The transition states in which the chlorines adopt a *trans* arrangement and the nucleophile is *trans* to the *N*-oxide (**BP2**) lie 2.5 kcal mol^{-1} (for *R*) and 3.8 kcal mol^{-1} (for *S*) *higher* in free energy than **BP1**(R). Finally, for all but two of the TSs with a *cis* arrangement of the chlorines (**BP3**−**BP10**) one or both of the *R* and *S* TSs are predicted to be lower in free energy than **BP2**; many are nearly equal in free energy to **BP1**.

Because of the multitude of low-lying transition states for this model system, these results indicate that no particular ligand configuration is preferred for general *N*-oxide catalysts. In other words, for realistic catalysts other subtle factors can easily tip the balance in favor of any one of these arrangements.

Although results for this model system indicate no preference for a particular ligand arrangement, the predicted free energy gaps between the *R* and *S* transition states for a given ligand arrangement provide a guideline for proposed transition state models for these catalysts. This is because this stereocontrolling center will play a dominant role in determining the overall selectivity of these types of catalysts. For example, the ligand arrangement in **BP2** is predicted to lead to a 1.3 kcal mol^{-1} preference for the TS leading to the *R*-product. Hence, unless there are other effects that can overcome this 1.3 kcal mol^{-1} bias toward *R*, this ligand configuration will lead to selective formation of the *R* enantiomer. For many of the other ligand arrangements this inherent stereoselectivity is even stronger, and must be considered in the development of transition state models for these reactions. As seen below for the helical *N*-oxide catalyst of Takenaka and co-workers,[5] the results depicted in Figure 1 provide qualitatively correct predictions of the free energy differences between the *R* and *S* transition states corresponding to a given ligand arrangement.

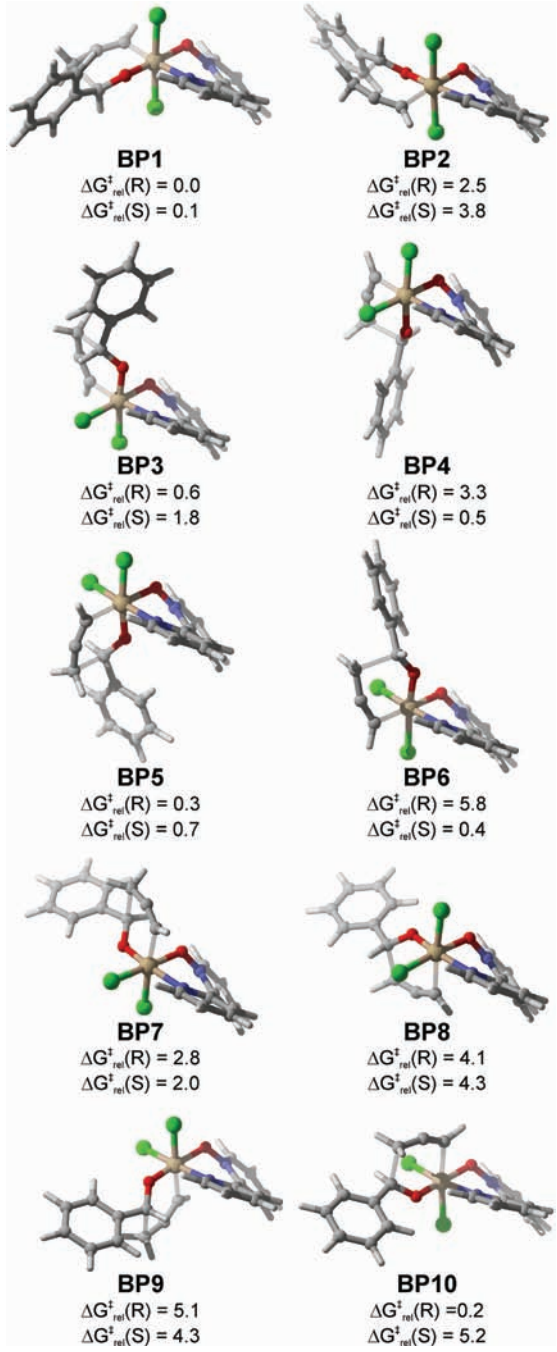

Figure 1. Transition states in dichloromethane for the model (*S*)-2,2′-bipyridine *N*-oxide catalyst, along with the relative free energy ($\Delta G^{\ddagger}_{rel}$, kcal mol^{-1}) for the TSs leading to the *R* (pictured) and *S* products. All of the free energies are relative to the lowest-lying **BP1**(R) structure. For each ligand arrangement, the corresponding *S* transition state is formed by simply rotating the aldehyde by ∼180° about the C═O bond.

3.2. Takenaka's Helical *N*-Oxide Catalyst. Having examined the possible ligand arrangements for a model bipyridine *N*-oxide catalyst, we now turn to the helical catalyst developed by Takenaka and co-workers.[5] Free energy differences for the two lowest-lying *S* and *R* transition states for the propargylation of benzaldehyde and several substituted benzaldehydes catalyzed by **1** are included in Table 1; free

dx.doi.org/10.1021/ja209241n | J. Am. Chem. Soc. 2012, 134, 3095−3102

Table 1. Free Energies of the Lowest-Lying R TS, Relative to the Lowest-Lying S TS ($\Delta G^{\ddagger}_{rel}$, kcal mol^{-1}), and Theoretical and Experimental ee's for the Propargylation of Selected Aromatic Aldehydes Catalyzed by 1 and 2[a]

cat.	Ar	$\Delta G^{\ddagger}_{rel}$	ee (theor)	ee (exp)
1	H-Ph	0.9	77	86
1	4-F-Ph	1.0	87	88
1	4-MeO-Ph	0.9	83	74
1	2-F-Ph	1.4	93	92
1	2-MeO-Ph	2.7	97	94
2	H-Ph	0.6	69	36

[a]See Table 2 and SI Figure S1 for free energies of other computed TSs. ee (theo) was calculated as described in Theoretical Methods and includes contributions from all TSs within 2 kcal mol^{-1} of the lowest lying TS.

Table 2. Relative Free Energy ($\Delta G^{\ddagger}_{rel}$) and Energy ($\Delta E^{\ddagger}_{rel}$) Barriers, and Relative Distortion and Interaction Energies (ΔE^{dist}_{rel} and ΔE^{int}_{rel}) for Key Transition States (see Figures 2 and 5)[a]

	$\Delta G^{\ddagger}_{rel}$	$\Delta E^{\ddagger}_{rel}$	ΔE^{dist}_{rel}	ΔE^{int}_{rel}
TS(S)/**1**	0.0	0.0	0.0	0.0
TS(R)/**1**	0.9	2.1	−1.6	3.7
TS(S′)/**1**	1.9	2.0	11.4	−9.4
TS(R′)/**1**	1.1	2.3	0.4	1.9
TS(S″)/**1**	3.6	4.1	7.3	−3.2
TS(R″)/**1**	3.2	2.7	1.3	1.4
Takenaka TS(R)/**1**	5.4	4.1	7.6	−3.5
Takenaka TS(S)/**1**	3.1	2.3	8.3	−6.0
TS(S)/**2**	0.0	0.0	0.0	0.0
TS(R)/**2**	1.6	2.3	−1.2	3.6
TS(S′)/**2**	−0.1	−0.5	4.8	−5.4
TS(R′)/**2**	0.6	0.7	−2.4	3.1
TS(S″)/**2**	2.5	2.2	2.7	−0.5
TS(R″)/**2**	0.7	0.0	−1.4	1.4
Takenaka TS(R)/**2**	3.6	2.2	5.4	−3.2
Takenaka TS(S)/**2**	1.7	−0.1	6.2	−6.2

[a]All data relative to either TS(S)/**1** or TS(S)/**2**.

energies for all other TSs are listed in SI Figure S1. Table 1 also includes experimental and predicted ee's. Overall, the theoretical predictions are in accord with experimental ee's. In particular, the predicted difference in free energy between the two lowest-lying *S* and *R* TSs for benzaldehyde, 0.9 kcal mol^{-1}, is in excellent agreement with the experimentally observed ee of 86%. Accounting for all thermodynamically accessible pathways, the predicted ee is decreased to 77%, which is still in reasonable agreement with experiment. The only qualitative discrepancy between the predicted and measured ee's occurs for *p*-methoxybenzaldehyde. In this case, B97-D predicts an enhanced enantioselectivity relative to benzaldehyde, but experimentally there is a 12% reduction in the ee. However, the difference in the predicted ee (83%) and the measured ee (74%) for 4-MeO-substituted benzaldehyde corresponds to an error in $\Delta\Delta G^{\ddagger}$ of only 0.15 kcal mol^{-1}.

Key low-lying *S* and *R* transition states for the propargylation of benzaldehyde catalyzed by **1** are depicted in Figure 2. Relative free energies and gas phase energies for these TSs are provided in Table 2 (free energies for other possible TSs are shown in SI Figure S1). The lowest-lying *S* and *R* TSs feature the aldehyde and allene *cis* to the *N*-oxide, and the two chlorines also in a *cis* arrangement. This ligand arrangement corresponds to model transition states **BP7** (see Figure 1). It is noteworthy that the gap between **BP7**(S) and **BP7**(R), 0.8 kcal mol^{-1}, is in excellent agreement with the predicted 0.9 kcal mol^{-1} free energy difference between TS(S)/**1** and TS(R)/**2**. Although for the other predicted TSs the agreement is not this good, there is qualitative agreement between the predictions from the model *N*-oxide catalyst and this helical catalyst (compare SI Figure S1 and Figure 1). In particular, for all but one of the ligand arrangements, the model *N*-oxide results indicate the correct selectivity for the *R* or *S* enantiomer for this helical catalyst. The only exception is the ligand arrangement in **BP8**, for which the model system predicts the *R* and *S* transition states to be roughly equal in free energy, while for the helical *N*-oxide catalyst B97-D predicts a 1.7 kcal mol^{-1} preference for *S*.

Also included in Figure 2 are transition states corresponding to the TS model of Takenaka et al. (Scheme 3).[5] Takenaka TS(R) is 2.3 kcal mol^{-1} lower in free energy than Takenaka TS(S), and hence, with this arrangement of ligands the predicted enantioselectivity is opposite to that observed experimentally. This is unsurprising in light of the results for the model catalyst examined above. This is because the ligand

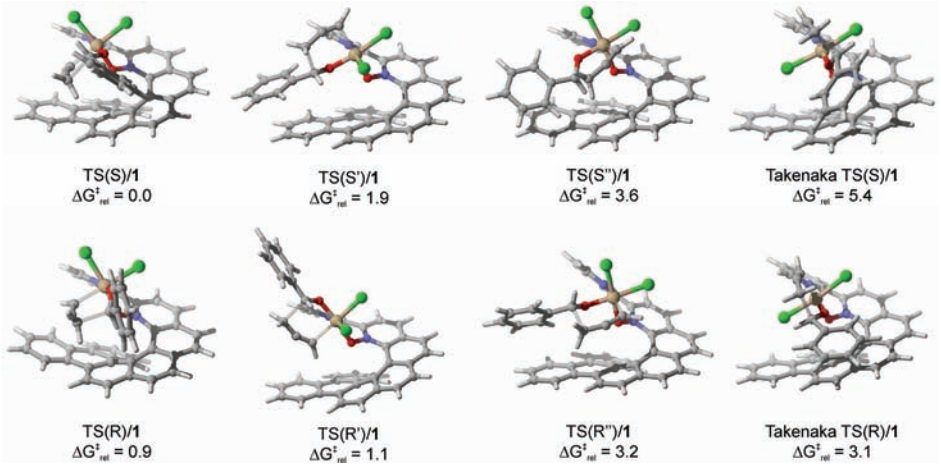

Figure 2. Key low-lying transition states for the propargylation of benzaldehyde catalyzed by **1**. Free energy barriers ($\Delta G^{\ddagger}_{rel}$, kcal mol^{-1}) are given relative to TS(S)/**1**. See SI for other low-lying transition states.

dx.doi.org/10.1021/ja209241n | *J. Am. Chem. Soc.* 2012, 134, 3095−3102

arrangement in Takenaka's TS model (**BP2**) leads to a 1.3 kcal mol^{-1} bias toward the *R* transition state. Apparently, inclusion of the helix in this catalyst shifts this balance more in favor of the *R* transition state. Moreover, Takenaka TS(S)/**1** and Takenaka TS(R)/**1** are predicted to be 5.4 and 3.1 kcal mol^{-1} higher in free energy than TS(S)/**1**, respectively, so are unlikely to play any role in this reaction.

In Table 2, it can be seen that relative gas phase energy barriers for catalyst **1** follow the same trends as the solution phase free energy barriers, indicating that solvent and entropy effects do not have a substantial net impact on the relative free energies of these transition states. As such, we focus below on relative gas phase energies, neglecting the impact of solvent and entropy. In this way, the selectivity for the *S* enantiomer, which arises primarily from the 0.9 kcal mol^{-1} free energy difference between TS(S)/**1** and TS(R)/**1**, can be explained in terms of the distortion of the reactants and inter- and intramolecular interactions.

In terms of gas-phase energies, TS(R)/**1** lies 2.1 kcal mol^{-1} higher than TS(S)/**1**. As seen in Table 2, distortion energies favor TS(R)/**1** over TS(S)/**1** by 1.6 kcal mol^{-1}. It is the difference in interaction energies, ΔE^{int}_{rel}, that results in TS(R)/**1** lying 2.1 kcal mol^{-1} higher in energy than TS(S)/**1**. In these transition states, E^{int} includes contributions from noncovalent interactions between the aldehyde and helix in addition to the usual covalent effects from the partially formed and broken bonds. The model systems depicted in Figure 3 were used to differentiate between these contributions to E^{int}. Here, the "aldehyde–catalyst" contribution was defined as the difference in energy between the complex of the aldehyde with the allenyltrichlorinesilane bound to the "core" of the catalyst (i.e., the black structure in Figure 3), and the separated aldehyde and trichlorosilane–catalyst adduct. Similarly, the "aldehyde–helix" contribution to E^{int} was determined from the relative energy of the aldehyde–helix complex and separated aldehyde and helix (red in Figure 3). In both cases, the positions of all conserved atoms were fixed, and only the added hydrogen atoms were optimized. These contributions to the energy gap between TS(R)/**1** and TS(S)/**1** are depicted in Figure 3. Remarkably, the aldehyde–catalyst interaction (+4.3 kcal mol^{-1}) strongly favors TS(S)/**1** over TS(R)/**1**, and the aldehyde–helix interactions actually reduce the energy difference between TS(R)/**1** and TS(S)/**1** by 1 kcal mol^{-1}. In other words, the energetic preference for *Si*-face attack over *Re*-face attack arises from favorable interactions between the aldehyde and the trichlorosilane–catalyst adduct *without the helix*. This effect is tempered by noncovalent interactions between the aldehyde and helix as well as the greater energy required to distort the reactants into the geometry of TS(S)/**1** compared to TS(R)/**1**.

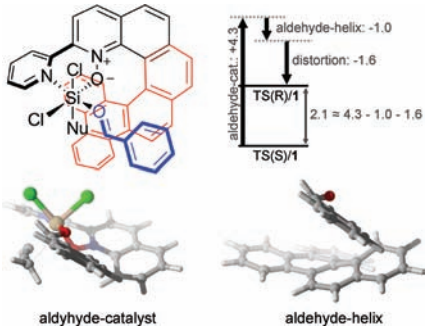

Figure 3. Model complexes used to approximately decompose the interaction energy (E^{int}, kcal mol^{-1}) into contributions from interactions of the aldehyde (blue) with the core of the catalyst (black) and the noncovalent interactions between the aldehyde (blue) and the helix (red), as applied to TS(S)/**1**. The contribution of E^{dist} and the aldehyde–catalyst and aldehyde–helix components of E^{int} to the *difference* in gas phase energies between TS(R)/**1** and TS(S)/**1** is depicted in the top right. There is a small degree of overcounting, which arises in part from the duplicated ethylene unit.

The 4.3 kcal mol^{-1} difference in the aldehyde-catalyst interaction for TS(S)/**1** and TS(R)/**1** can be rationalized in part by considering the atomic charges and interatomic distances in these transition states. As seen in Figure 4, the carbonyl carbon, which bears a charge of ~0.25*e*, is 0.77 Å closer to the negatively charged Cl *trans* to the *N*-oxide in TS(S)/**1** than it is in TS(R)/**1**, and is equidistant from the other Cl. This leads to a net electrostatic stabilization of TS(S)/**1** over TS(R)/**1**. Such effects will be general for *N*-oxide catalysts based on alkyltrichlorosilanes adopting the **BP7** arrangement of ligands.

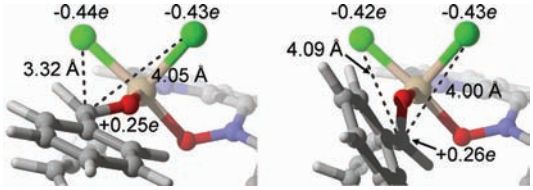

Figure 4. Selected atomic charges (NPA)[25] and distances between the carbonyl carbon and Cl ligands in TS(S)/**1** (left) and TS(R)/**1** (right).

In Takenaka's TS model, it was proposed that *Re*-face attack was hindered by steric interactions between the aldehyde and the terminal benzo ring of the helix (see Scheme 3). This proposal was bolstered by the significant reduction in enantioselectivity observed for catalyst **2** compared to **1**. However, from the optimized structure of Takenaka TS(R)/**1**, the closest contact between the aldehyde and the terminal benzo ring of the helix is 4.6 Å, precluding any steric interactions. Hence, there must be an alternative explanation for the marked difference in selectivity between catalysts **1** and **2**.

Transition states for the propargylation of benzaldehyde catalyzed by **2** were optimized in order to explain the reduced stereoselectivity. Key low-lying TSs are depicted in Figure 5. As with catalyst **1**, for **2** it was found that TS(S)/**2** is low-lying. However, in the case of catalyst **2**, there is an additional predicted transition state, TS(S′)/**2**, which is essentially isoergonic with TS(S)/**2**. More importantly, there are two low-lying *R* TSs. These transition states, TS(R′)/**2** and TS(R″)/**2**, are only 0.6 and 0.7 kcal mol^{-1} higher in free energy than TS(S)/**2**, and are responsible for the reduced enantioselectivity of catalyst **2**. For catalyst **1**, TS(R′)/**1** and TS(R″)/**1** are much higher-lying. The reason TS(R′)/**2** and TS(R″)/**2** are so low-lying is that less energy is required to distort the reactants into the TS geometries than for TS(S)/**2**. This effect cancels the effect of E^{int}, which favors TS(S)/**2**. This is the opposite effect as was observed for catalyst **1**, for which both E^{int} and E^{dist} favor TS(S)/**1**. For example, for catalyst **2** the contribution of distortion (−1.4 kcal mol^{-1}) and interaction (+1.4 kcal mol^{-1}) to the energy difference between TS(R″)/**2** and TS(S)/**2** exactly cancel, leading to equal gas-phase energies for these two transition states. For catalyst **1**, the distortion (+1.3 kcal mol^{-1})

dx.doi.org/10.1021/ja209241n | *J. Am. Chem. Soc.* 2012, 134, 3095–3102

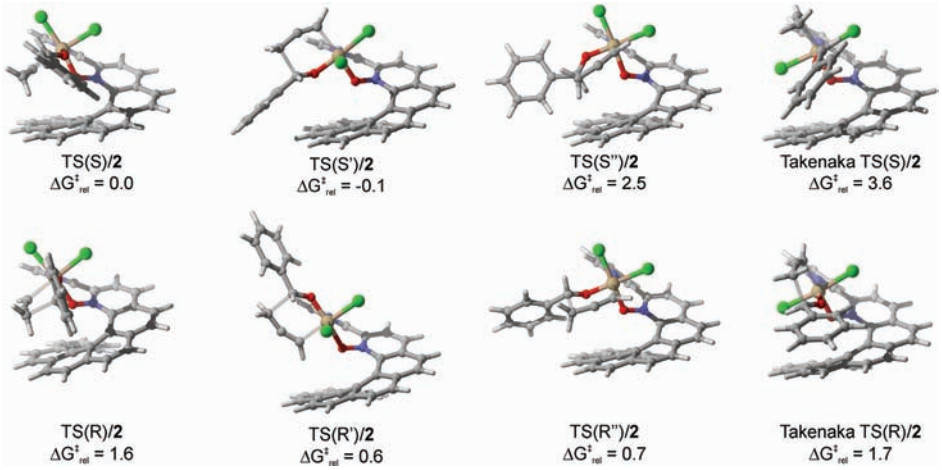

Figure 5. Key low-lying transition states for the propargylation of benzaldehyde catalyzed by **2**. Free energy barriers ($\Delta G^{\ddagger}_{rel}$, kcal mol^{-1}) are given relative to TS(S)/**2**.

and interaction (+1.4 kcal mol^{-1}) add to yield the 2.7 kcal mol^{-1} energy difference between TS(R″)/**1** and TS(S)/**1**.

4. SUMMARY AND CONCLUSIONS

The enantioselective propargylation of aromatic aldehydes with allenyltrichlorosilane catalyzed by 2,2′-bipyridine *N*-oxides has been investigated using DFT. (*S*)-2,2′-bipyridine *N*-oxide was studied as a model catalyst in order to examine the dependence of predicted relative free energy barriers on the arrangement of ligands around the hexacoordinate silicon. This model study yielded two primary conclusions. First, there is no strong preference for a given arrangement of ligands about the stereocontrolling hexacoordinate silicon transition state, and for a given *N*-oxide catalyst the preferred ligand arrangement will depend on other factors (steric and other noncovalent interactions, etc.). Second, because the different ligand arrangements around the hexacoordinate silicon lead to drastically different stereochemical outcomes for these reactions, the present results provide guidelines for proposed TS models. In particular, many ligand arrangements result in a strong bias toward formation of either the *R* or *S* homopropargylic alcohol, even in the absence of other chiral elements. This inherent selectivity will be a major determinant of the overall enantioselectivity of *N*-oxide propargylation catalysts. It was shown that for a given ligand arrangement, these model computations provide qualitatively correct predictions of selectivities for the helical *N*-oxide catalyst of Takenaka and co-workers.[5]

For this helical *N*-oxide catalyst of Takenaka and co-workers, the present theoretical predictions are in accord with experimental observations,[5] and provide a simple explanation for the observed enantioselectivities. The present results support the TS model depicted in Scheme 4, which is also consistent with available experimental data[5] as well as results from the model *N*-oxide catalyst. However, this TS model is different from that previously published by Takenaka and co-workers (see Scheme 3).[5] Most notably, in the TS model in Scheme 4 the chlorines adopt a *cis* arrangement, and the allenyl group is *cis* to the *N*-oxide; in Takenaka's TS model both of these arrangements are *trans*. The present results point to simple electrostatic interactions between the carbonyl group of the aldehyde and the silyl chlorines as the dominant determinant of selectivity. These electrostatic effects outweigh

Scheme 4. Proposed Transition Model Based on the Present Computational Data (Nu = allene)

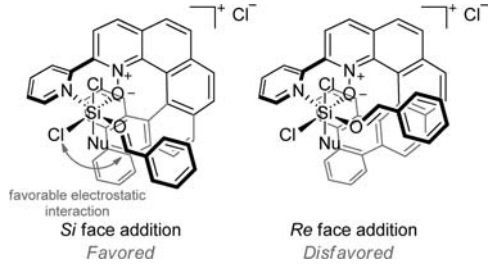

the impact of stabilizing noncovalent aryl−aryl interactions between the aldehyde and the helix. Aryl−aryl interactions stabilize the R transition state, and actually reduce the selectivity of these reactions.

Although the helical catalyst of Takenaka[5] is a covalent catalyst, the high degree of enantioselectivity is a result of stabilizing noncovalent interactions. This is in line with the enzyme-inspired catalyst design principles recently outlined by Knowles and Jacobsen.[2] In this case it is simple electrostatic interactions that stabilize the preferred pathway, not π-stacking interactions or hydrogen bonds. As discussed above, however, the aryl−aryl interactions of the aldehyde with the helix reduce the free energy difference between the lowest-lying *S* and *R* transition states, and therefore, this catalyst does not achieve maximal selectivity. Ongoing efforts are aimed at refining this catalyst to stabilize the preferred pathway through electrostatic and π-stacking interactions acting in concert to achieve enhanced enantioselectivity.

■ ASSOCIATED CONTENT

Supporting Information

Complete citation for ref 22; absolute energies and computed free energies; Cartesian coordinates and figures for computed transition states.This material is available free of charge via the Internet at http://pubs.acs.org.

■ AUTHOR INFORMATION

Corresponding Author

wheeler@chem.tamu.edu

■ ACKNOWLEDGMENTS

This work was supported in part through The Welch Foundation, Grant A-1775. We thank the Texas A&M Supercomputing Facility for providing computational resources and Dr. Elango Munusamy for helpful comments. Molecular figures were generated using CYLView.[26]

■ REFERENCES

(1) (a) List, B.; Yang, J. W. *Science* **2006**, *313*, 1584−1586. (b) Dalko, P. I.; Moisan, L. *Angew. Chem., Int. Ed.* **2004**, *43*, 5138−5175. (c) Carpenter, J.; Northrup, A. B.; Chung, D.; Miener, J. J. M.; Kim, S.-G.; MacMillan, D. W. C. *Angew. Chem., Int. Ed.* **2008**, *47*, 3568−3572. (d) Dondoni, A.; Massi, A. *Angew. Chem., Int. Ed.* **2008**, *47*, 4638−4660.

(2) Knowles, R. R.; Jacobsen, E. N. *Proc. Natl. Acad. Sci. U.S.A.* **2010**, *107*, 20678−20685.

(3) (a) Wheeler, S. E.; Houk, K. N. *J. Am. Chem. Soc.* **2008**, *130*, 10854−10855. (b) Wheeler, S. E.; Houk, K. N. *Mol. Phys.* **2009**, *107*, 749−760. (c) Wheeler, S. E.; Houk, K. N. *J. Chem. Theory Comput.* **2009**, *5*, 2301−2312. (d) Wheeler, S. E.; McNeil, A. J.; Müller, P.; Swager, T. M.; Houk, K. N. *J. Am. Chem. Soc.* **2010**, *132*, 3304−3311. (e) Bloom, J. W. G.; Wheeler, S. E. *Angew. Chem., Int. Ed.* **2011**, *50*, 7847−7849. (f) Raju, R. K.; Bloom, J. W. G.; An, Y.; Wheeler, S. E. *ChemPhysChem* **2011**, *21*, 3116−3130. (g) Wheeler, S. E. *J. Am. Chem. Soc.* **2011**, *133*, 10262−10274.

(4) Cheong, P. H.-Y.; Legault, C. Y.; Um, J. M.; Çelebi-Olçüm, N.; Houk, K. N. *Chem. Rev.* **2011**, *111*, 5042−5137.

(5) Takenaka, N.; Chen, J. S.; Captain, B. *Org. Lett.* **2011**, *13*, 1654−1657.

(6) (a) Marshall, J. A. *Chem. Rev.* **1996**, *96*, 31−47. (b) Marshall, J. A. *J. Org. Chem.* **2007**, *72*, 8153−8166.

(7) (a) Kobayashi, S.; Nishio, K. *J. Am. Chem. Soc.* **1995**, *117*, 6392−6393. (b) Shimada, T.; Kina, A.; Ikeda, S.; Hayashi, T. *Org. Lett.* **2002**, *4*, 2799−2801. (c) Shimada, T.; Kina, A.; Hayashi, T. *J. Org. Chem.* **2003**, *68*, 6329−6337. (d) Malkov, A. V.; Bell, M.; Vassieu, M.; Bugatti, V.; Kocovsky, P. *J. Mol. Catal. A: Chem.* **2003**, *196*, 179−186. (e) Malkov, A. V.; Dufkova, L.; Farrugia, L.; Kocovsky, P. *Angew. Chem., Int. Ed.* **2003**, *42*, 3674−3677. (f) Chelucci, G.; Murineddu, G.; Pinna, G. A. *Tetrahedron Asymmetry* **2004**, *15*, 1373−1389. (g) Pignataro, L.; Benaglia, M.; Cinquini, M.; Cozzi, F.; Celentano, G. *Chirality* **2005**, *17*, 396−403. (h) Malkov, A. V.; Bell, M.; Castelluzzo, F.; Kočovský, P. *Org. Lett.* **2005**, *7*, 3219−3222. (i) Orito, Y.; Nakajima, M. *Synthesis (Stuttgart)* **2006**, 1391−1401. (j) Schneider, U.; Sugiura, M.; Kobayashi, S. *Adv. Synth. Catal.* **2006**, *348*, 323−329. (k) Schneider, U.; Sugiura, M.; Kobayashi, S. *Tetrahedron* **2006**, *62*, 496−502. (l) Malkov, A. V.; Kocovsky, P. *Eur. J. Org. Chem.* **2007**, 29−36. (m) Benaglia, M.; Guizzetti, S.; Pignataro, L. *Coord. Chem. Rev.* **2008**, *252*, 492−512. (n) Hrdina, R.; Boyd, T.; Valterova, I.; Hodacova, J.; Kotora, M. *Synlett* **2008**, 3141−3144. (o) Malkov, A. V.; Ramirez-Lopez, P.; Biedermannova, L.; Rulisek, L.; Dufkova, L.; Kotora, M.; Zhu, F. J.; Kocovsky, P. *J. Am. Chem. Soc.* **2008**, *130*, 5341−5348. (p) Malkov, A. V.; Westwater, M. M.; Gutnov, A.; Ramirez-Lopez, P.; Friscourt, F.; Kadlcikova, A.; Hodacova, J.; Rankovic, Z.; Kotora, M.; Kocovsky, P. *Tetrahedron* **2008**, *64*, 11335−11348. (q) Curtis-Long, M. J.; Aye, Y. *Chem.—Eur. J.* **2009**, *15*, 5402−5416. (r) Kadlcikova, A.; Hrdina, R.; Valterova, I.; Kotora, M. *Adv. Synth. Catal.* **2009**, *351*, 1279−1283. (s) Malkov, A. V.; Kabeshov, M. A.; Barlog, M.; Kocovsky, P. *Chem.—Eur. J.* **2009**, *15*, 1570−1573. (t) Vlasana, K.; Hrdina, R.; Valterova, I.; Kotora, M. *Eur. J. Org. Chem.* **2010**, 7040−7044. (u) Kadlcikova, A.; Valterova, I.; Duchackova, L.; Roithova, J.; Kotora, M. *Chem.—Eur. J.* **2010**, *16*, 9442−9445. (v) Fulton, J. R.; Glover, J. E.; Kamara, L.; Rowlands, G. J. *Chem. Commun.* **2011**, *47*, 433−435. (w) Malkov, A. V.; Barlog, M.; Jewkes, Y.; Mikusek, J.; Kocovsky, P. *J. Org. Chem.* **2011**, *76*, 4800−4804. (x) Bergbreiter, D. E.; Ortiz-Acosta, D. *Tetrahedron Lett.* **2008**, *49*, 5608−5610.

(8) (a) Denmark, S. E.; Coe, D. M.; Pratt, N. E.; Griedel, B. D. *J. Org. Chem.* **1994**, *59*, 6161−6163. (b) Denmark, S. E.; Fu, J. P. *J. Am. Chem. Soc.* **2000**, *122*, 12021−12022. (c) Denmark, S. E.; Fu, J. P. *J. Am. Chem. Soc.* **2001**, *123*, 9488−9489. (d) Denmark, S. E.; Wynn, T. *J. Am. Chem. Soc.* **2001**, *123*, 6199−6200. (e) Denmark, S. E.; Fu, J. P. *Chem. Rev.* **2003**, *103*, 2763−2793. (f) Denmark, S. E.; Pham, S. M.; Stavenger, R. A.; Su, X. P.; Wong, K. T.; Nishigaichi, Y. *J. Org. Chem.* **2006**, *71*, 3904−3922. (g) Denmark, S. E.; Fu, J. P.; Coe, D. M.; Su, X. P.; Pratt, N. E.; Griedel, B. D. *J. Org. Chem.* **2006**, *71*, 1513−1522. (h) Denmark, S. E.; Beutner, G. L. *Angew. Chem., Int. Ed.* **2008**, *47*, 1560−1638.

(9) Nakajima, M.; Saito, M.; Hashimoto, S. *Tetrahedron Asymmetry* **2002**, *13*, 2449−2452.

(10) Nakajima, M.; Saito, M.; Hashimoto, S. *J. Am. Chem. Soc.* **1998**, *120*, 6419−6420.

(11) (a) Bahmanyar, S.; Houk, K. N. *J. Am. Chem. Soc.* **2001**, *123*, 12911−12912. (b) Allemann, C.; Gordillo, R.; Clemente, F.; Cheong, P. H.-Y.; Houk, K. N. *Acc. Chem. Res.* **2004**, *37*, 558−569. (c) Clemente, F.; Houk, K. N. *Angew. Chem., Int. Ed.* **2004**, *43*, 5766−5768. (d) Roy, D.; Sunoj, R. B. *Org. Lett.* **2007**, *9*, 4873−4876. (e) Houk, K. N.; Cheong, P. H.-Y. *Nature* **2008**, *455*, 309−313. (f) Fleming, E. M.; Quigley, C.; Rozas, I.; Connon, S. J. *J. Org. Chem.* **2008**, *73*, 948−956. (g) Shinisha, C. B.; Sunoj, R. B. *Org. Biomol. Chem.* **2008**, *6*, 3921−3929. (h) Sunoj, R. B. *WIREs Comp. Mol. Sci.* **2011**, *1*, 920−931.

(12) (a) Chen, J. S.; Takenaka, N. *Chem.—Eur. J.* **2009**, *15*, 7268−7276. (b) Takenaka, N.; Sarangthem, R. S.; Captain, B. *Angew. Chem., Int. Ed.* **2008**, *47*, 9708−9710. (c) Takenaka, N.; Chen, J. S.; Captain, B.; Sarangthem, R. S.; Chandrakumar, A. *J. Am. Chem. Soc.* **2010**, *132*, 4536−4537.

(13) (a) Nakajima, M.; Saito, M.; Shiro, M.; Hashimoto, S. *J. Am. Chem. Soc.* **1998**, *120*, 6419−6420. (b) Hrdina, R.; Opekar, F.; Roithová, J.; Kotora, M. *Chem. Commun.* **2009**, 2314−2316. (c) Chelucci, G.; Belmonte, N.; Benaglia, M.; Pignataro, L. *Tetrahedron Lett.* **2007**, *48*, 4037−4041. (d) Sereda, O.; Tabassum, S.; Wilhelm, R. *Top. Curr. Chem.* **2010**, *291*, 349−393.

(14) (a) Musher, J. I. *Angew. Chem., Int. Ed. Engl.* **1969**, *8*, 54−68. (b) Tandura, S. N.; Voronkov, M. G.; Alekseev, N. V. *Top. Curr. Chem.* **1986**, *131*, 99−189.

(15) (a) Malkov, A. V.; Orsini, M.; Pernazza, D.; Muir, K. W.; Langer, V.; Meghani, P.; Kocovsky, P. *Org. Lett.* **2002**, *4*, 1047−1049. (b) Malkov, A. V.; Bell, M.; Orsini, M.; Pernazza, D.; Massa, A.; Herrmann, P.; Meghani, P.; Kocovsky, P. *J. Org. Chem.* **2003**, *68*, 9659−9668. (c) Traverse, J. F.; Zhao, Y.; Hoveyda, A. H.; Snapper, M. L. *Org. Lett.* **2005**, *7*, 3151−3154.

(16) Denmark, S. E.; Fan, Y.; Eastgate, M. D. *J. Org. Chem.* **2005**, *70*, 5235−5248.

(17) Schenker, S.; Schneider, C.; Tsogoeva, S. B.; Clark, T. *J. Chem. Theory Comput.* **2011**, *7*, 3586−3595.

(18) (a) Grimme, S. *J. Comput. Chem.* **2006**, *27*, 1787−1799. (b) Becke, A. *J. Chem. Phys.* **1997**, *107*, 8554−8560. (c) Schafer, A.; Huber, C.; Ahlrichs, R. *J. Chem. Phys.* **1994**, *100*, 5829−5835. (d) Dunning, T. H. Jr. *J. Chem. Phys.* **1989**, *90*, 1007−1023.

(19) Grimme, S. *WIREs Comp. Mol. Sci.* **2011**, *1*, 211−228.

(20) Goerigk, L.; Grimme, S. *Phys. Chem. Chem. Phys.* **2011**, *13*, 6670−6688.

(21) (a) Tomasi, J.; Mennucci, B.; Cammi, R. *Chem. Rev.* **2005**, *105*, 2999−3093. (b) Miertus, S.; Scrocco, E.; Tomasi, J. *Chem. Phys.* **1981**, *55*, 117−129.

(22) Frisch, M. J.; et al.. *Gaussian 09*, Revision B.01; Gaussian, Inc.: Wallingford CT, 2009.

(23) (a) Ess, D. H.; Houk, K. N. *J. Am. Chem. Soc.* **2007**, *129*, 10646−10647. (b) Legault, C. Y.; Garcia, Y.; Merlic, C. A.; Houk, K. N. *J. Am. Chem. Soc.* **2007**, *129*, 12664−12665. (c) Ess, D. H.; Houk, K. N. *J. Am. Chem. Soc.* **2008**, *130*, 10187−10198. (d) Lam, Y. H.; Cheong, P. H. Y.; Blasco Mata, J. M.; Stanway, S. J.; Gouverneur, V.; Houk, K. N. *J. Am. Chem. Soc.* **2009**, *131*, 1947−1957. (e) Hayden, A. E.; Houk, K. N. *J. Am. Chem. Soc.* **2009**, *131*, 4084−4089. (f) Cheong, P. H. Y.; Paton, R. S.; Bronner, S. M.; Im, G. Y. J.; Garg, N. K.; Houk, K. N. *J. Am. Chem. Soc.* **2010**, *132*, 1267−1268. (g) Paton, R. S.; Kim,

S.; Ross, A. G.; Danishefsky, S. J.; Houk, K. N. *Angew. Chem., Int. Ed.* **2011**, *50*, 10366−10368.
(24) (a) Bickelhaupt, F. M.; van Zeist, W. J. *Org. Biomol. Chem.* **2010**, *8*, 3118−3127. (b) Bickelhaupt, F. M. *J. Comput. Chem.* **1999**, *20*, 114−128.
(25) Foster, J. P.; Weinhold, F. *J. Am. Chem. Soc.* **1980**, *102*, 7211−7218.
(26) Legault, C. Y. *CYLview*, 1.0b; Université de Sherbrooke: Quebec, Canada, 2009 (http://www.cylview.org).